Week 7 – Submarine Pyroclastic Activity

(there was no lecture for week 6)

Note: some of these slides were provided by Dave Clague, MBARI

Two topics:

“fluidal” clasts and bubble wall fragments – internal water or steam production?

Gas driven eruptions: dissolved gas chemistry and the formation of fragmentary pyroclast deposits

Depth – pressure relationships
100m = 11 bar
1000m = 101 bar
4000m = 403 bar

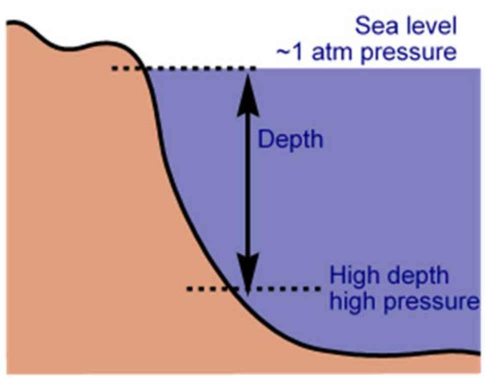

http://www.calctool.org/CALC/other/games/depth_press

“fluidal” clasts and bubble wall fragments

Issues: *Internal vs external driving force*

is there enough internal water in submarine magmas, especially MORB?

To what depth can external water be converted to reasonable quantities of steam?

How does this happen?

Estimates of volatile contents of MORBS and some ocean island basaltic magmas

Volatile Contents in Tholeiites

Sample	CO_2	H_2O	Reference
EMORB Popping Rocks	0.8-1	-	Gerlach, 1991
EMORB Popping Rocks	0.75	0.58	Graham and Sarda, 1991
EMORB Popping Rocks	0.79	0.59	this study
NMORB Gorda T196 (a)	0.75	~0.16	this study
Kilauea Primary Magma	0.70	0.37	Clague et al. 1991, Gerlach et al., 2002
Loihi 6.93%MgO tholeiite (b)	0.82	0.59	this study
Loihi Primary Tholeiite (16.5% MgO)	0.62	0.44	this study

(a) assumes 95% vesicle gas is CO_2, H_2O_m=K_2O=0.09, CO_{2m}=0.02
(b) assumes 80% vesicle gas is CO_2, H_2O_m=0.51, CO_{2m}=67 ppm (Dixon)

Clague et al., 2000

Post entrapment modification of melt inclusions – Wallace, 2005

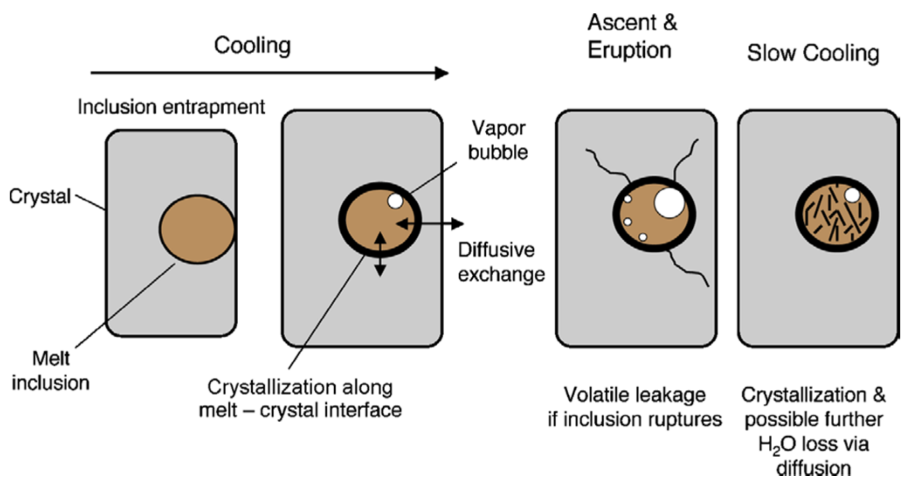

Loihi Seamount with locations where limu o Pele was recovered in pushcores, scoops and small sediment dredges

Clague et al., 2000

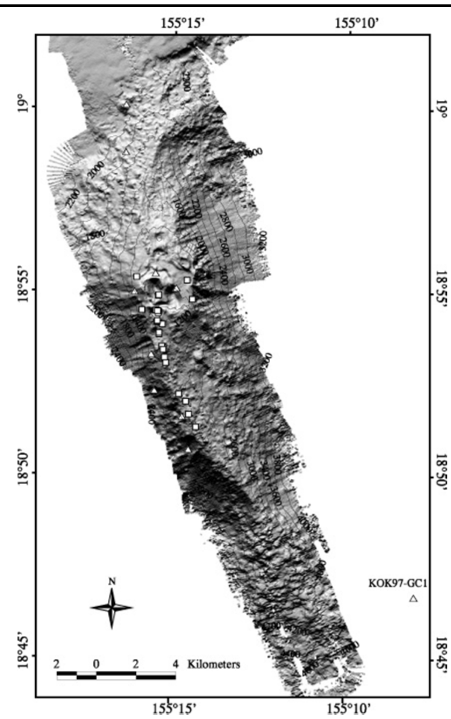

Typical fragments of limu o Pele from Loihi's summit, largest grains are about 4 mm across. Right shows typical Pele's hair fragments from Loihi.

Loihi Seamount pyroclastic fragments – Clague et al., 2000

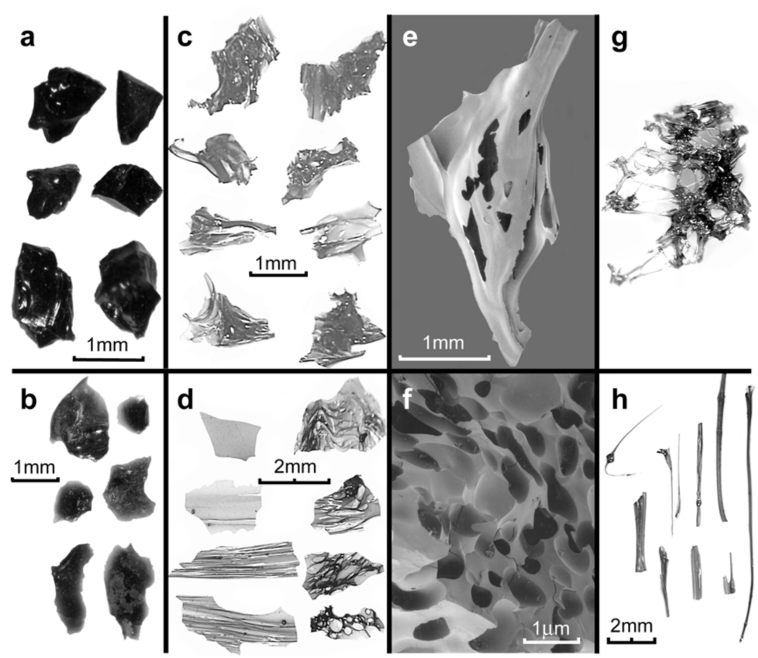

Gorda Ridge location map,

with Tiburon ROV dive locations in red. (slide from dave)

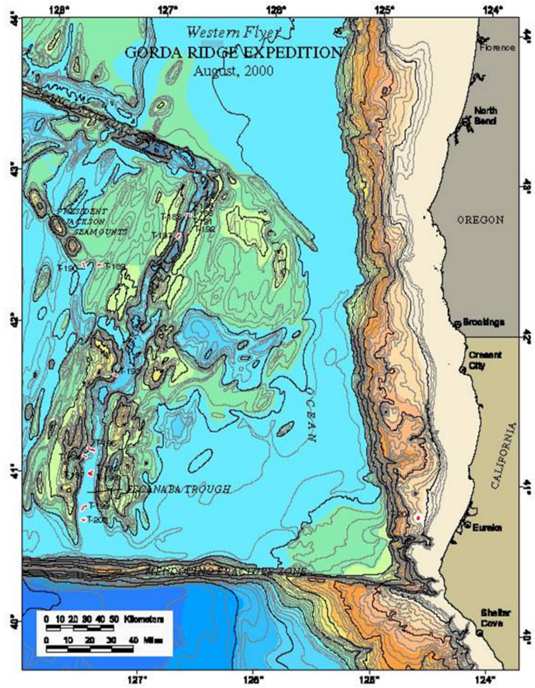

One way to sample pyroclastic particulates is to push-core. We also use a small suction sampler and literally vacuum the bottom on flows where there is little sediment.

A variety of pyroclastic fragments recovered from the Gorda Ridge

SEM images of Gorda Ridge fragments

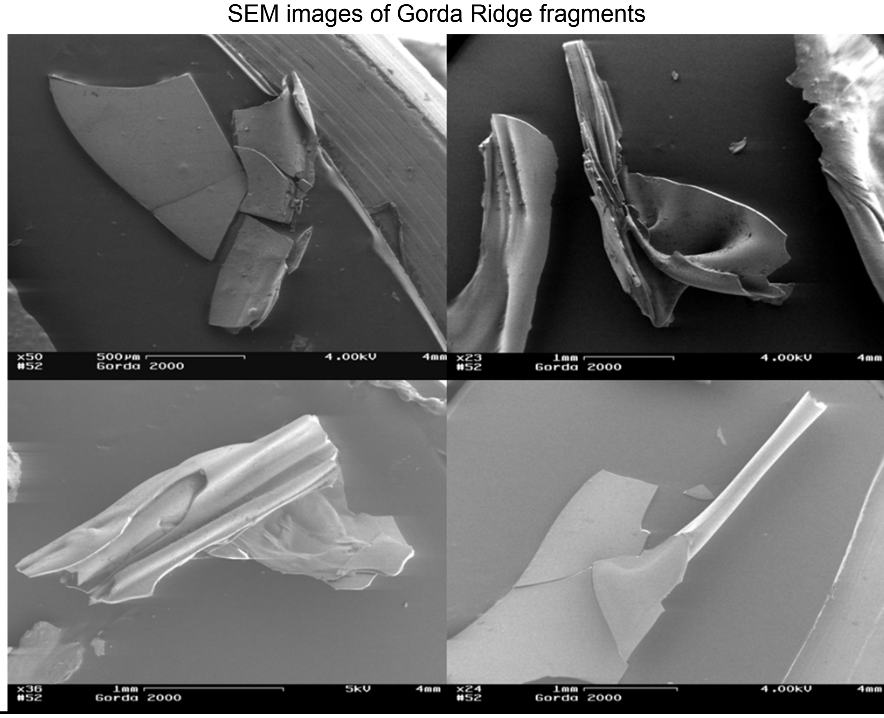

More SEM images of Gorda Ridge fragments

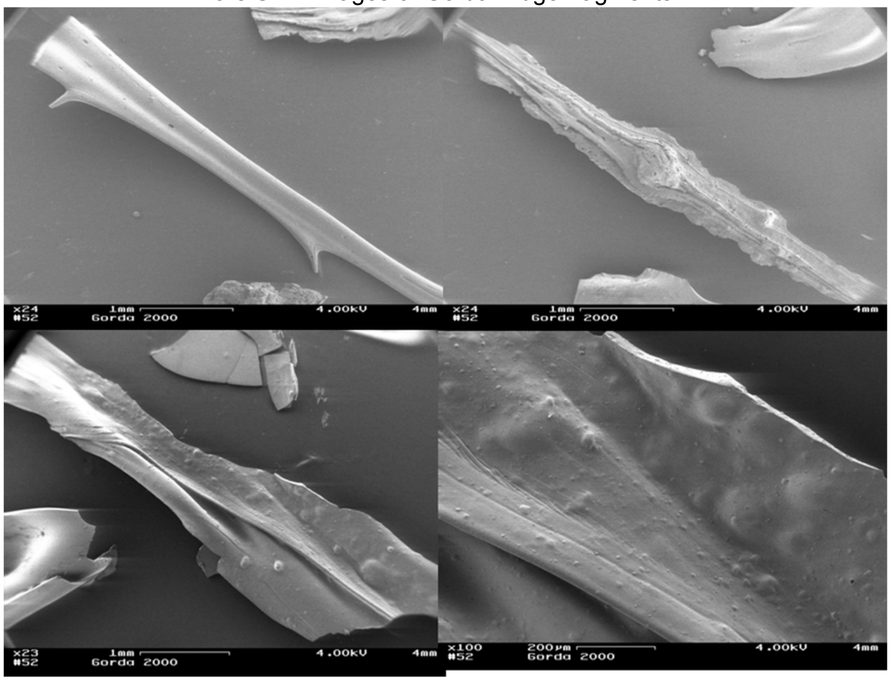

specific volume of combined solid (halite=H) liquid (L) and water vapor (V) as a function of temperature at various pressures. Figure 9, Clague et al. (2000)

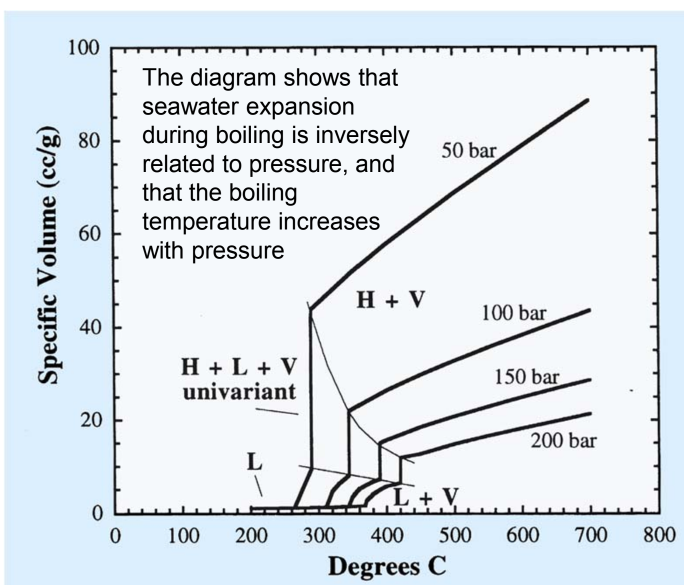

Fig. 8, Clague et al., 2000

A. Plot of CO2 vs H2O for seven limu o Pele fragments from Loihi Seamount compared with several Lo'ihi Seamount pillow rinds. The limu o Pele fragments have CO2 and H2O contents comparable to those of the pillow-rind glasses, supporting the interpretation that the limu o Pele fragments have experienced little to no loss of H2O due to degassing.

B. Pressure of equilibration, based on CO2 and water contents and solubilities, vs pressure of collection for a selection of limu o Pele fragments.

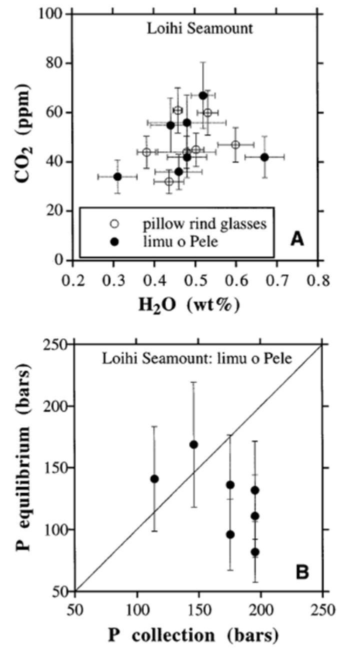

Maicher and White, 2003.

Limu-bearing sheet hyaloclastite was formed at depths of 1400–2000 m bsl at Seamount Six (near the EPR at 12 N).

Hyaloclastites there are non-vesicular, supersaturated with CO2 and show only a slight degassing trend of H2O.

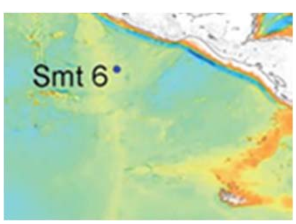

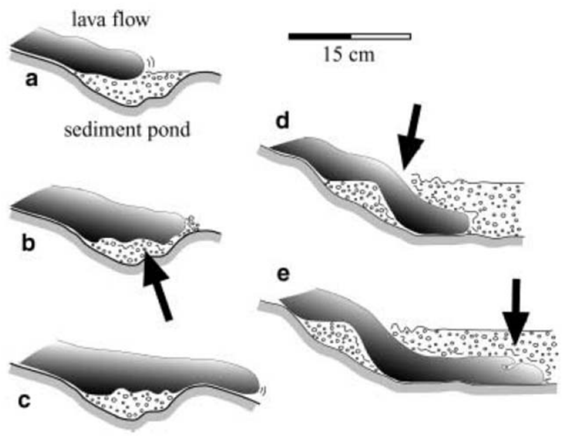

Fig. 4a–e Submarine sheet lava flowing onto a sediment-filled pond. **a–c** Thin flow, supported by sediment, covers a small pond and displaces some material, developing an irregular base; or **d** sediment failure after fluidisation beneath lava, lava sinks into the sediment and continues to flow beneath it, continuously fluidising and vaporising the wet sediment (*arrow*), sediment entrapment of initially supporting sediment, **e** sediment entrapment in flow vugs near the flow front (*arrow*)

Maicher and White, 2003.

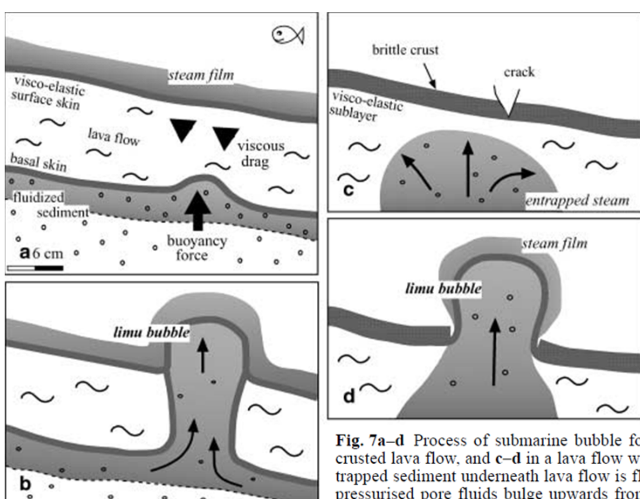

Fig. 7a–d Process of submarine bubble formation **a–b** in an uncrusted lava flow, and **c–d** in a lava flow with a brittle crust. **a** Entrapped sediment underneath lava flow is fluidised, vaporised, and pressurised pore fluids bulge upwards from the substrate-lava interface into lava, driven by buoyancy force and balanced by viscous drag force of lava and visco-elastic surface skin. Note entrained sediment. **b** Diapiric rise of steam bulge to stretch the visco-elastic layers into a limu bubble skin. A steam film protects the forming bubble. **c** A lava flow with a rigid, brittle upper surface crust and visco-elastic sublayer with steam trapped and ponding beneath the crust (either individual steam bubble or larger steam reservoir), in which crack formation occurs, penetrating the brittle crust downwards into the visco-elastic sublayer. **d** Steam bulge breaches through crack, stretching the visco-elastic sublayer into a limu bubble with a protecting steam film

Maicher and White, 2003.

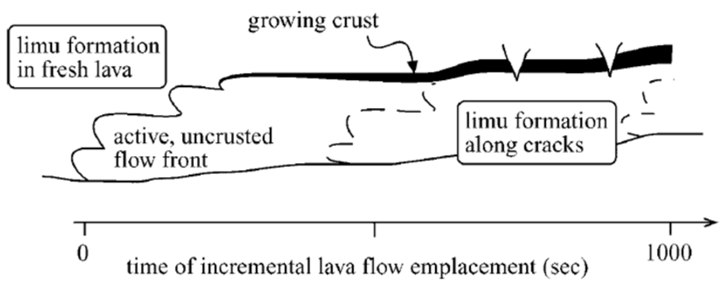

Fig. 8 Position of limu formation sites in both the active, uncrusted lava flow front and through newly formed cracks in older crust

Maicher and White, 2003.

Maicher and White, 2003.

The most common way to make limu is by water and/or water saturated sediment trapped in extremely thin, fluid and rapidly advancing lava flows by various processes.

Bubble formation might also occur by these mechanisms…

(a) small-scale magma-fountaining driven by magmatic volatile exsolution
and
(b) extreme vent constriction or during collapse of pillows and rapid drainage of the magma.

Gas driven eruptions:

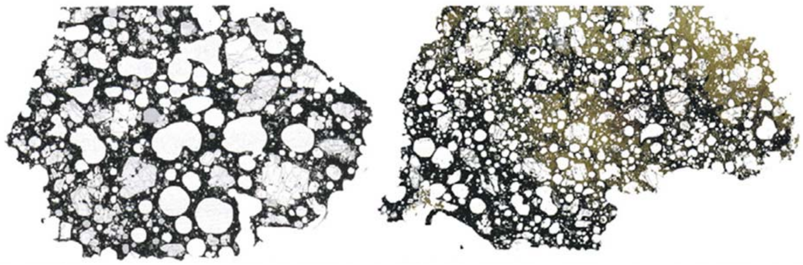

Two vesicular clast types from Loihi,
Schipper et al., 2011

dissolved gas chemistry and the formation of fragmentary pyroclast deposits

Deep pyroclast formation requires that these eruptions be driven by juvenile (magmatic) volatiles.

How the magma evolves in P-T-composition space and when it looses its gases will play a major role in the types of deposits that are formed.

Pulsed, Strombolian, eruption of partly to mostly degassed clasts appears to be most common.

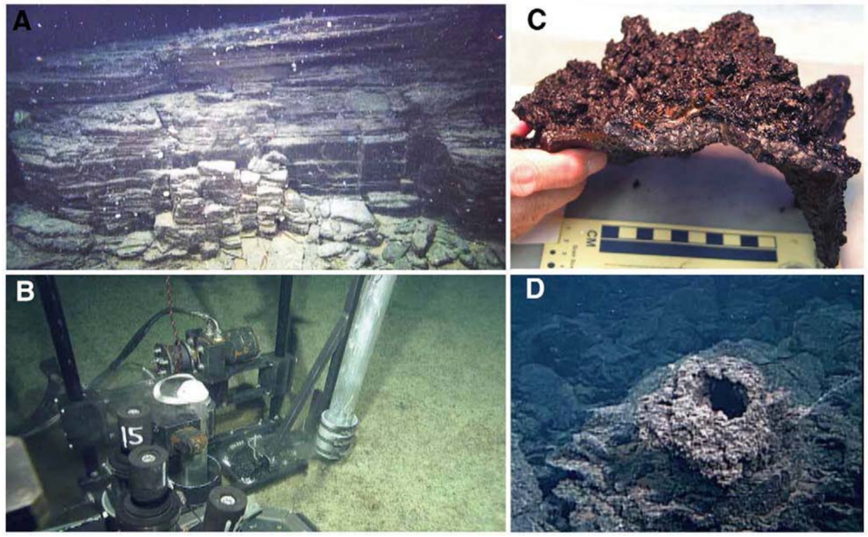

Fig. 8. A) Lithified 2-m thick hyaloclastite deposit on one of the Vance Seamounts photographed during dive T1011. B) Unconsolidated glassy sands on the northeast rim of Axial Volcano on the Juan de Fuca Ridge. The metal frame attached to the ROV Tiburon is a 2-m vibracorer showing a core inserted into the bottom the full 2-m length (the core top is just to the right of the #15 pushcore handle). A spare core tube is carried on the front edge of the vibracorer. C) A rock of agglutinated spatter collected from a lava pond complex on the south rift of Axial Volcano. D) The small hornito-like vent structure sampled in C. The mound is about 1 m in diameter. Clague et al., 2009

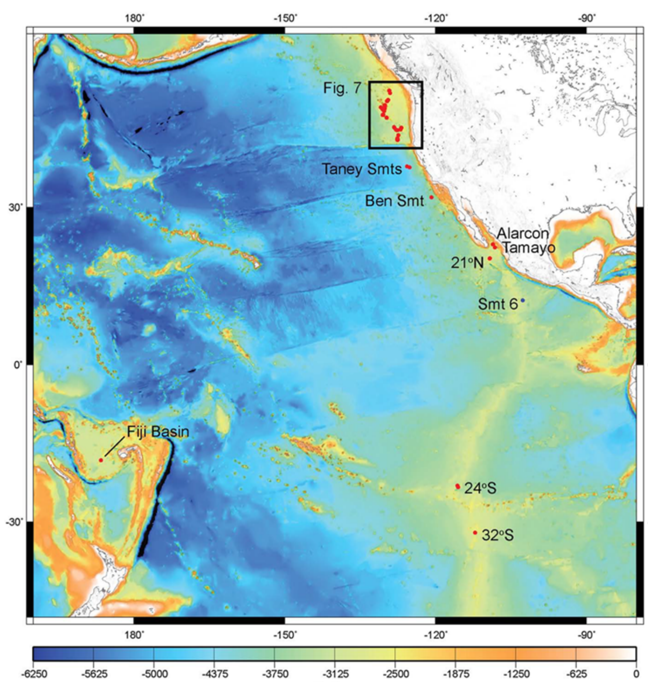

Fig. 6. Bathymetric map of the Pacific Ocean showing the 467 sites in red where we have collected pyroclastic glass fragments (data from Appendix A). The sites are described in the text. The lone blue sample is the location of Seamount 6 from the literature (e.g., Maicher and White, 2001). The box shows the region expanded in Fig. 7.

Clague et al., 2009

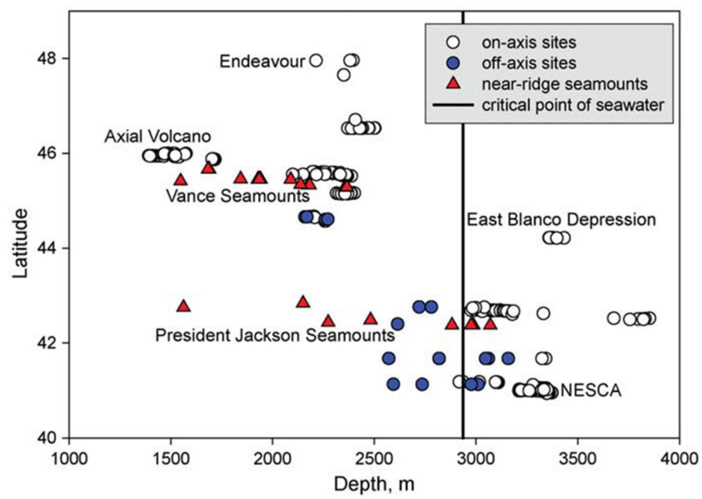

Fig. 9. Depth plotted against latitude for the samples with volcanic glass fragments from the region shown in Fig. 7. The vertical line denotes the critical point of seawater; sites at greater depth cannot produce steam by boiling seawater. Nearly all the sites along the Gorda Ridge are from below this critical depth.

Clague et al., 2009

Fragmentation (that) occurs at pressures above the critical point of seawater cannot be caused by a phase change of seawater to steam. The fragments are of pyroclastic origin, most likely erupted during strombolian bubble burst activity.

Clague et al., 2009

So is this driven by water vapor or CO2?

H2O vs. CO2 variations during formation of differentiated magma from basaltic parents (B) by vapor-saturated fractional crystallization at 2, 3, and 5 kb pressure. Approximately 60–70% fractional crystallization is necessary to drive residual liquids from an initial H2O of 2.25 to 4–5 wt.% (i.e., values found in many explosive subaerial magmas).

The degassing curve shows the path for magma formed by closed-system fractional crystallization at 5 kb.

P.J. Wallace / Journal of Volcanology and Geothermal Research 140 (2005) 217–240

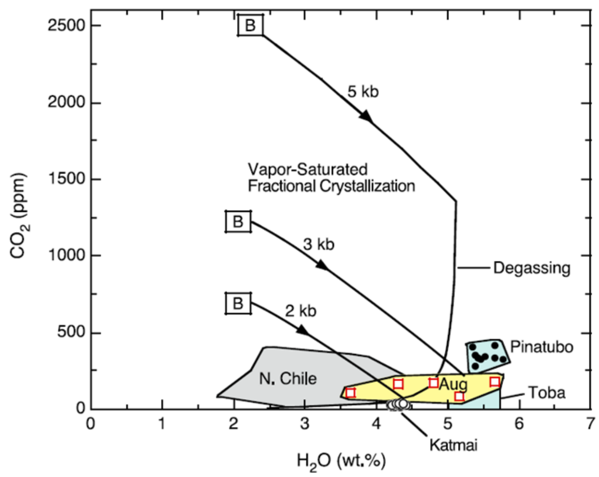

During isobaric fractional crystallization of vapor-saturated magma, H2O increases in the residual liquid, but CO2 is preferentially lost to the vapor phase because of its lower solubility. Significant amounts of H2O will not be degassed from such differentiating magmas until CO2 is largely degassed from the melt, at which point the melt becomes saturated with nearly pure H2O vapor.

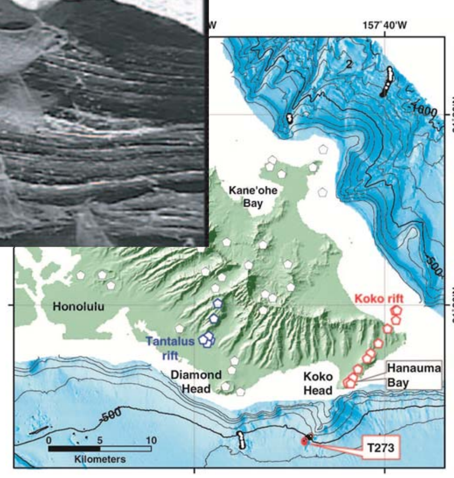

Cross-bedded fine volcanic ash beds near collection site of T273-R8 at 513 m.
Clague et al., 2006

Summit of Loihi showing Pele's Pit, which formed in 1996. Summit collapse events maybe be accompanied by widespread pyroclastic eruptions.

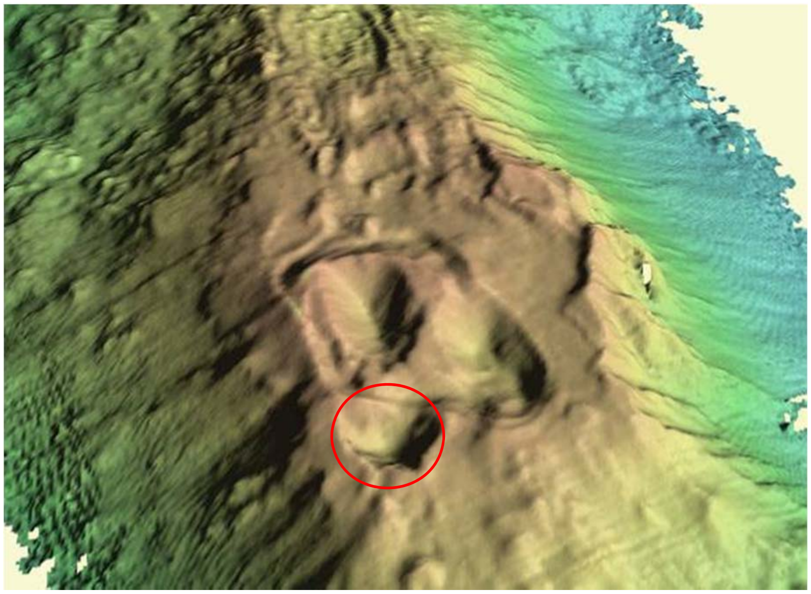

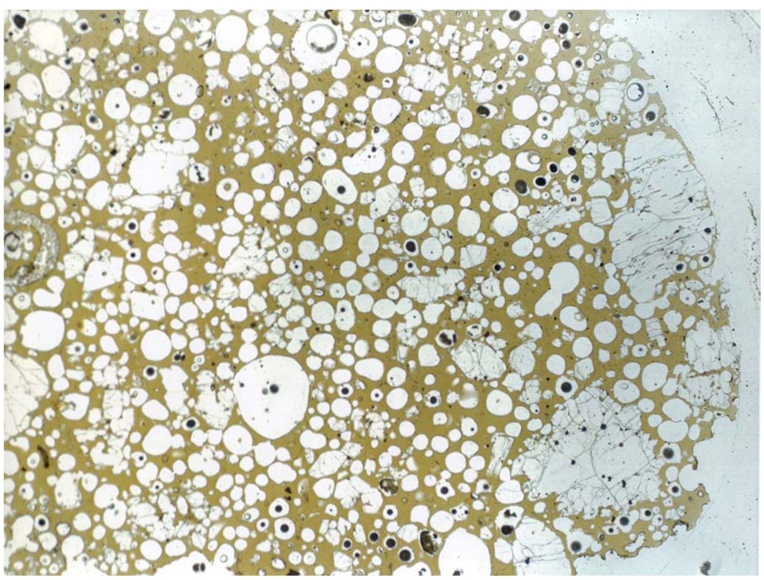

Highly vesicular Loihi Seamount tholeiitic lava from upper south Rift Zone (this one with 53.6% glass, 25.3% bubbles, and 21.1% olivine). Such lavas demonstrate the high magmatic gas content of Loihi tholeiites.

(Slide from Dave Clague)

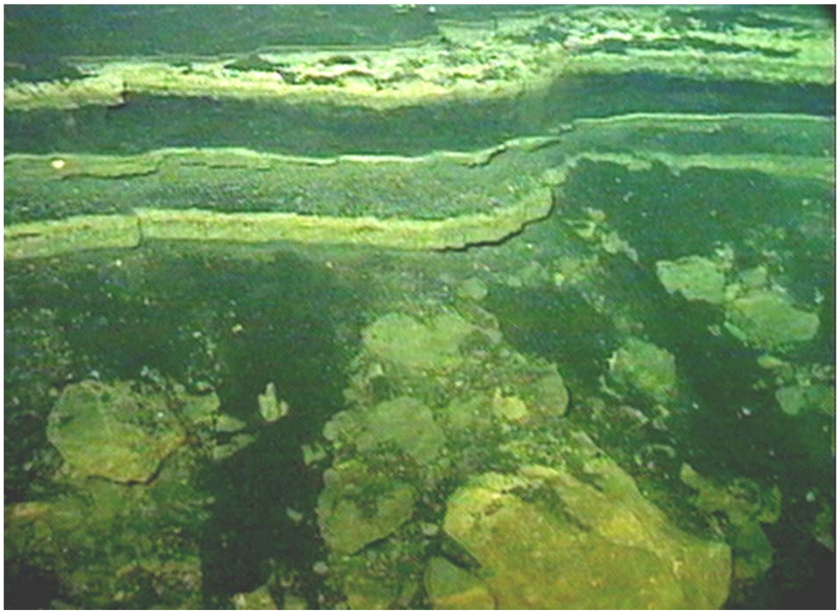

Upper part of 11-m section of clastic deposits on summit of Loihi. Lighter colored layers are finer grained (more clay and silt) than dark layers which are sands and gravels.

(Slide from Dave Clague)

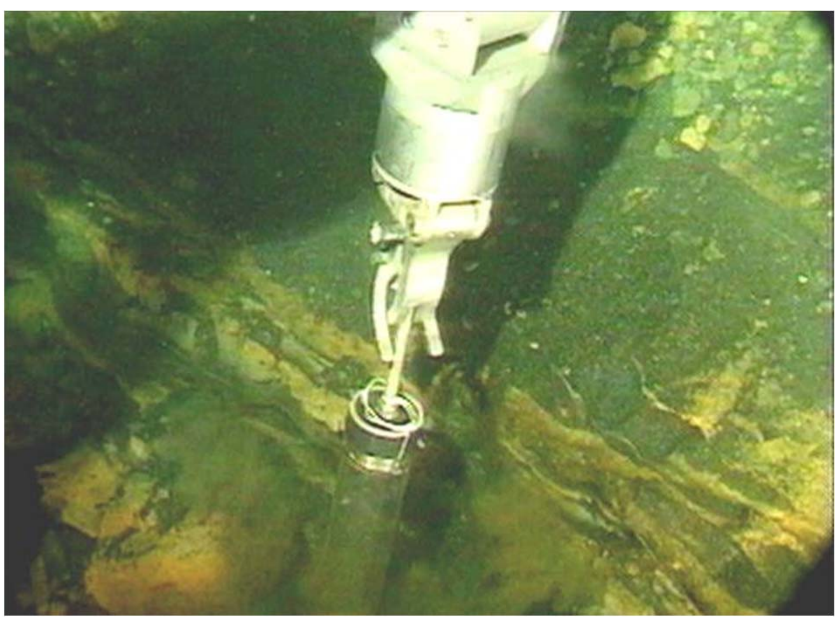

Sampling the same 11-m section. Results published in Clague et al. (2003)

(Slide from Dave Clague)

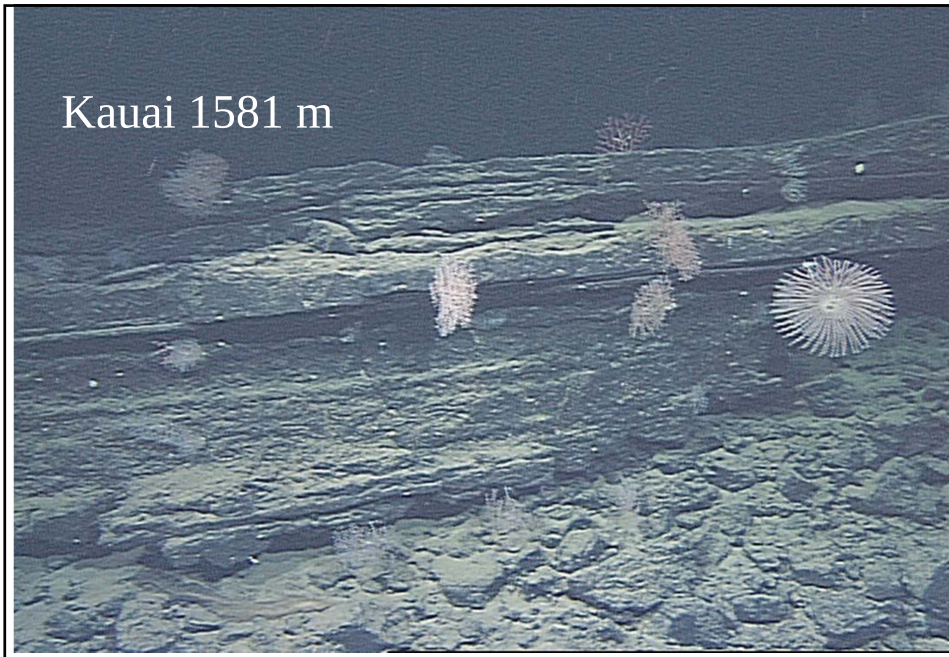

Bedded ash deposits on south flank of Kauai.

(Slide from Dave Clague)

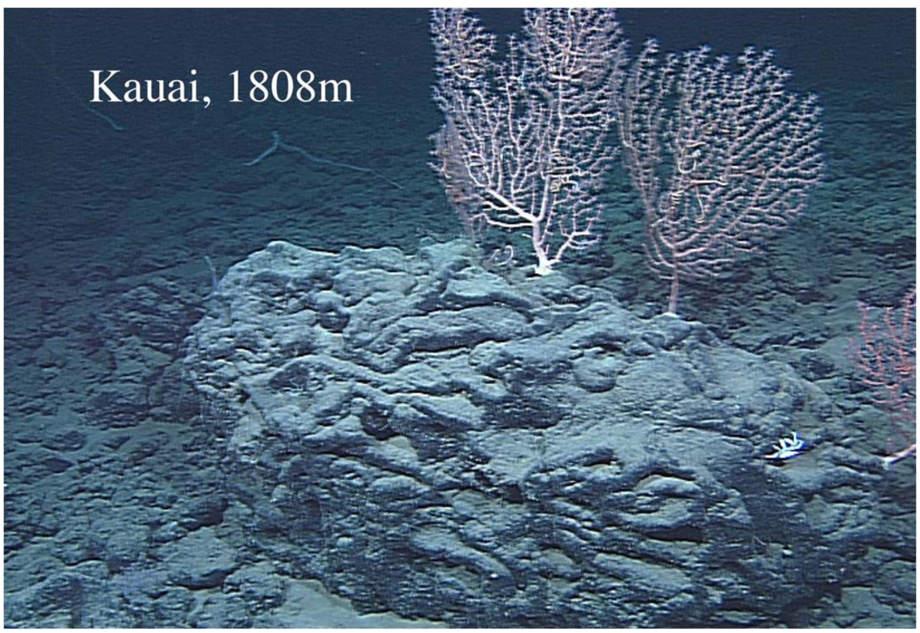

Agglutinated spatter at submarine rejuvenated stage vent on south flank of Kauai.

(Slide from Dave Clague)

Thin outcrop of volcanic ash on the west flank of the Gorda Rift Valley. Particles have local MORB compositions. *(Slide from Dave Clague)*

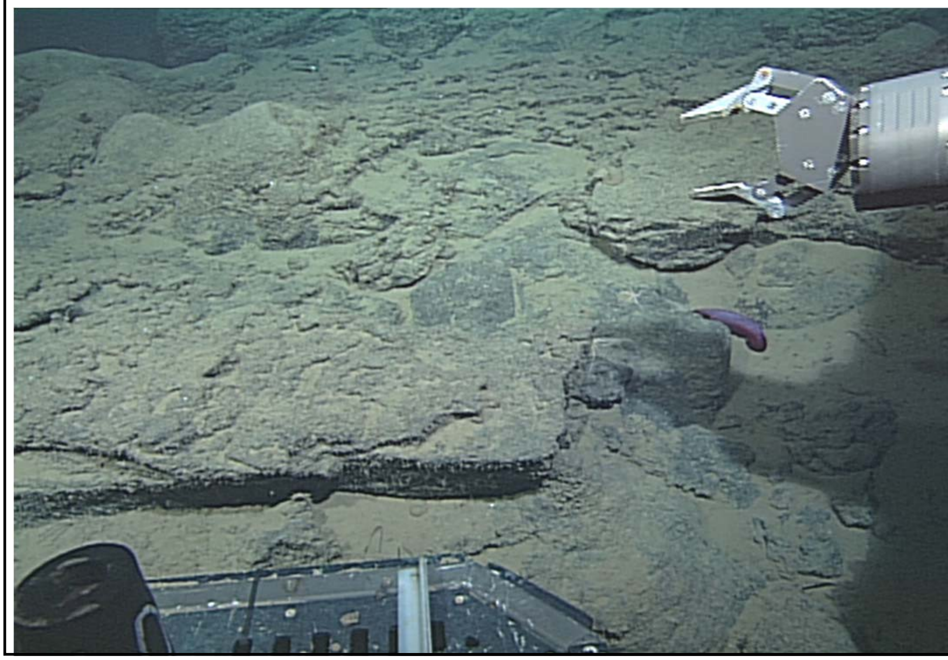

"… in the magma chamber and during eruption, MORB will lose a part or nearly all of its original gas, because without the development of a separate volatile rich zone in the magma chamber, no eruption takes place."

Bottinga and Javoy, 1989

"Strombolian activity is most likely caused by addition of magmatic foam from the top of the magma reservoir to resident magma."

Clague et al., 2009

Loihi revisited:

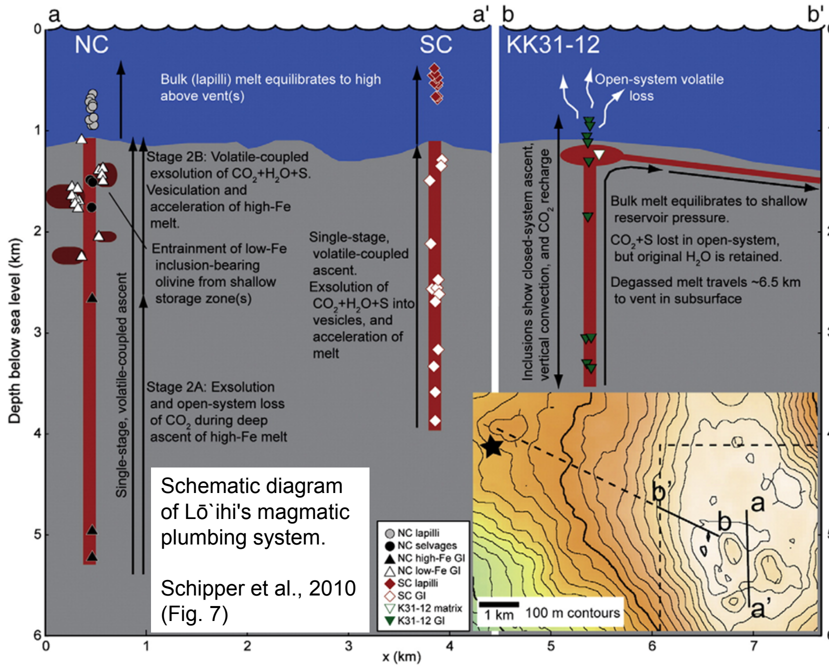

Schematic diagram of Lō`ihi's magmatic plumbing system.

Schipper et al., 2010 (Fig. 7)

Sulfur and water degassing systematics. Schipper 2010 Fig. 5.

A: S vs. FeT for matrix glasses and inclusions from the northern cone (symbols), the southern cone (grey fields), and KK31-12 (hatched fields and upside down triangle), plotted against the MORB FeS saturation curve (Dixon et al., 1991). Note that all matrix glasses plot below the saturation curve, indicating that they have degassed S, and high-Fe northern cone inclusions form a continuous trend in decreasing S toward matrix glasses.

B: S vs. H2O, symbols as in A. Note general correlation of decreasing S and H2O from inclusions to matrix glasses in the northern and southern cone, but not in KK31-12.

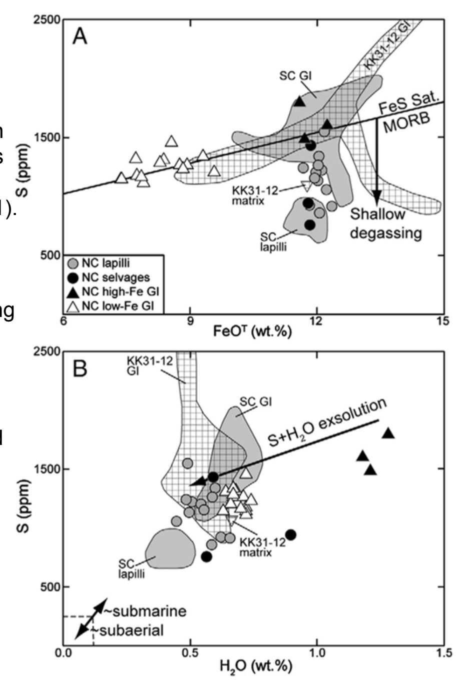

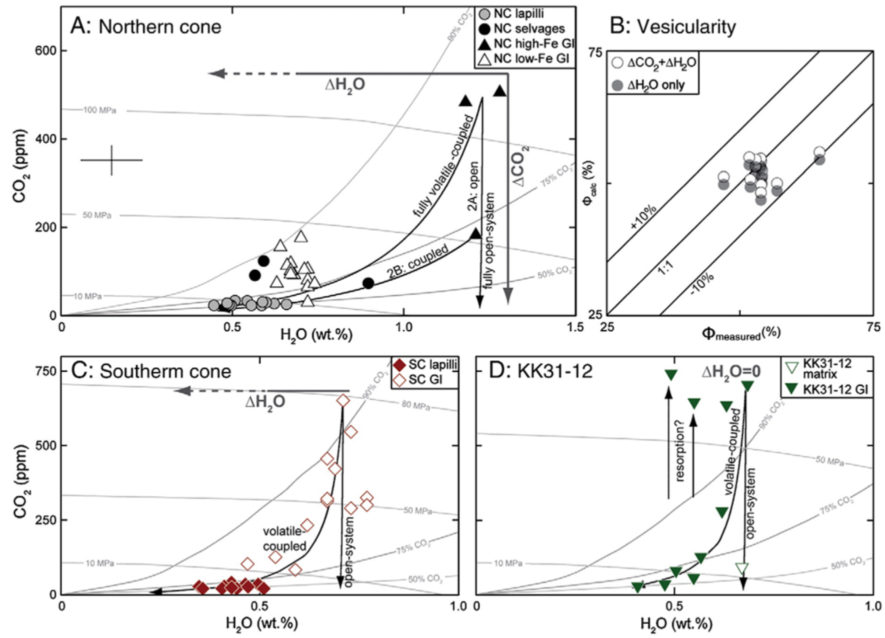

CO_2 and H_2O exsolution at Lō`ihi. Schipper et al., 2010 (Fig. 6)

Stratigraphy and clast density of a pyroclastic deposit at Loihi.

Schipper et al., 2011 (Fig. 2)